# Optimized Spectral Fault Receptive Fields for Diagnosis-Informed Prognosis

Stan Muñoz Gutiérrez¹ ⊠ ©

Institute of Software Engineering and Artificial Intelligence, Graz University of Technology, Austria

Franz Wotawa<sup>2</sup> 

□

Institute of Software Engineering and Artificial Intelligence, Graz University of Technology, Austria

#### Abstract

This paper introduces Spectral Fault Receptive Fields (SFRFs), a biologically inspired technique for degradation state assessment in bearing fault diagnosis and remaining useful life (RUL) estimation. Drawing on the center-surround organization of retinal ganglion cell receptive fields, we propose a frequency-domain feature extraction algorithm that enhances the detection of fault signatures in vibration signals. SFRFs are designed as antagonistic spectral filters centered on characteristic fault frequencies, with inhibitory surrounds that enable robust characterization of incipient faults under variable operating conditions. A multi-objective evolutionary optimization strategy based on NSGA-II algorithm is employed to tune the receptive field parameters by simultaneously minimizing RUL prediction error, maximizing feature monotonicity, and promoting smooth degradation trajectories. The method is demonstrated on the XJTU-SY bearing run-to-failure dataset, confirming its suitability for constructing condition indicators in health monitoring applications. Key contributions include: (i) the introduction of SFRFs, inspired by the biology of vision in the primate retina; (ii) an evolutionary optimization framework guided by condition monitoring and prognosis criteria; and (iii) experimental evidence supporting the detection of early-stage faults and their precursors. Furthermore, we confirm that our diagnosis-informed spectral representation achieves accurate RUL prediction using a bagging regressor. The results highlight the interpretability and principled design of SFRFs, bridging signal processing, biological sensing principles, and data-driven prognostics in rotating machinery.

2012 ACM Subject Classification Computing methodologies  $\rightarrow$  Causal reasoning and diagnostics; General and reference  $\rightarrow$  Reliability; Computing methodologies  $\rightarrow$  Genetic algorithms; Computing methodologies  $\rightarrow$  Machine learning; Hardware  $\rightarrow$  Failure prediction

Keywords and phrases Health Perception, Spectral Fault Receptive Fields, Remaining Useful Life, Incipient Fault Diagnosis, Prognostics and Health Management, Condition Monitoring, Evolutionary Multi-Objective Optimization, Bagged Regression Tree Ensemble, Bearing Fault Diagnosis

Digital Object Identifier 10.4230/OASIcs.DX.2025.9

Related Version Previous Version: https://doi.org/10.48550/arXiv.2506.12375

Supplementary Material

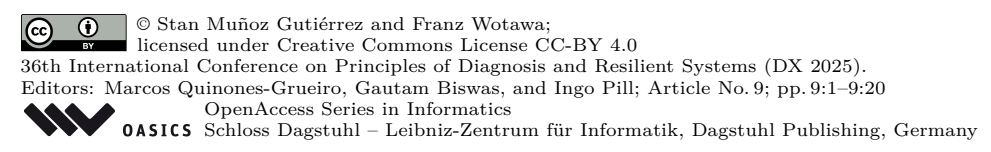
 $Software~(MATLAB~Notebook):~ \verb|https://doi.org/10.5281/zenodo.15660819~[24]|\\ Other~(Poster):~ \verb|https://doi.org/10.5281/zenodo.17141147|$ 

**Funding** This study was conducted within the framework of the ARCHIMEDES project, which is supported by the Chips Joint Undertaking and its members, including top-up funding from National Authorities under Grant Agreement No. 101112295 and the FFG under Grant Agreement No. FO999899377.



**Acknowledgements** SMG thanks Mike Denham for introducing him to the Biology of Vision and Ian Parmee for introducing him to Evolutionary Multi-Objective Engineering Design.

<sup>&</sup>lt;sup>2</sup> Corresponding author



Authors are listed in alphabetical order.

# 1 Introduction

In modern engineering, reliability is a central concern, distinguished from quality by its emphasis not only on compliance with specifications at "time zero," but also on sustained performance throughout an artifact's operational life. Central to reliability is the assessment and modeling of degradation rates and time to failure [19]. Reliability pertains to the performance and operation of systems and their components, aiming to deliver solutions that can operate without failure, nor be the cause of failure, over a specified time horizon and in accordance with specifications that define both constraints and operational conditions.

Rotary machines are ubiquitous in industrial and transportation contexts. Bearings, as key components of these machines, play a crucial role in ensuring reliable operation. Accurately estimating the degradation state of bearings throughout their operational life is essential for rational decision-making by both humans and automated systems. Such decisions include scheduling maintenance actions, investigating accelerated degradation trends, predicting component failure times, implementing closed-loop control for safety and energy efficiency, and, when done effectively, extending component lifetimes through feedback-driven control based on degradation state estimation.

As part of Project Archimedes, we investigate intelligent, data-driven methods for precise degradation state estimation and remaining useful life prediction, aiming to support decisions that extend the operational lifespan of electric vehicle powertrains (EVPs). A significant challenge in this research area is that existing knowledge on bearing diagnostics primarily pertains to bearings operating under constant conditions, which does not reflect the dynamic speed and load variations encountered in electric vehicle drives amid disturbances and aleatoric uncertainties. Although our study does not explicitly address these dynamic conditions, our approach is designed to integrate such parameters, whose implications we briefly discuss. Another critical challenge is the limited availability of open datasets; currently, only a few datasets capture run-to-failure data for electric drive components, which constrains research progress. For this study, we utilize the XJTU-SY dataset [36], one of the few publicly available run-to-failure datasets for rolling element bearings, to validate our proposed methods.

The work presented in this paper focuses on bearings, which are integral to the mechanisms that connect the electric drive to the transmission and enable vehicle propulsion. However, we have developed our model to be generalizable to some extent, making it potentially applicable to other aspects of the electric drive, such as electric winding faults, irreversible demagnetization of permanent magnets, and inverter degradation dynamics, assuming suitable adaptations are implemented.

Our work introduces a novel technique based on consolidated knowledge within the field of vibration analysis. Although many recent research efforts adopt tabula rasa methodologies, bypassing established domain knowledge in favor of black-box systems that often achieve high performance, these solutions frequently lack transparency and interpretability. In safety-critical domains such as electric drives, transparency is essential; certification requires that system behavior be understandable and trustworthy.

Our method, named Spectral Fault Receptive Fields, offers an interpretable technique to degradation state estimation, with condition indicators that correspond directly to specific failure modes in bearings. We evaluated the system primarily using the monotonicity criterion, and further incorporated smoothness and remaining useful life (RUL)-based metrics for parameter selection. Through qualitative comparison, we demonstrated clear improvements resulting from explicit multi-objective optimization of several system parameters, thereby validating the effectiveness of the approach.

This paper is organized to guide the reader through the development and validation of our approach. In Section 2, we review related work in diagnostics, prognostics, and health monitoring of engineered systems. Section 3 introduces the problem domain and dataset used for experimental evaluation. Section 4 details the design of Spectral Fault Receptive Fields (SFRFs), inspired by biological vision, as a novel feature extraction method for condition monitoring and remaining useful life prediction. Section 5 presents empirical evaluations and multi-objective optimization results demonstrating the proposed method's effectiveness. The discussion in Section 6 reflects on the biological foundations, parameter tuning, and future research directions. Finally, Section 7 concludes the paper by summarizing key contributions and implications for predictive maintenance.

# 2 Related Work

Traditionally, reliability assessments were based primarily on empirical field data derived statistically [5, 18]. These approaches were typically static, focused solely on random failures, often neglected underlying failure mechanisms, did not account for differences among vendors or specific devices in lifetime predictions, and excluded real-time condition monitoring [18]. In contrast, modern diagnostics and prognostics frameworks emphasize continuous degradation monitoring of components and systems. They employ a range of modeling strategies, including failure progression rates, physics-of-failure, statistical and probabilistic methods, and modeling of failure propagation between interconnected subsystems. This entails a more comprehensive and dynamic assessment of system health [35]. When the primary focus is on selecting optimal maintenance actions, predictive maintenance (PdM) serves as an appropriate conceptual framework. However, research in this area typically concentrates on two aspects, which are seldom addressed simultaneously: (1) predicting the time to failure, referred to as remaining useful life (RUL) prediction, and (2) optimizing maintenance strategies. Prognostics and health management (PHM) is conducive to informed decision-making and actions to keep systems in optimal operating condition. PHM is an integrated, modular process that includes system analysis, data acquisition, data processing, fault detection, fault diagnostics, failure prognostics, decision making, and maintenance scheduling [34]. A typical predictive maintenance workflow consists of the following steps: (1) data acquisition and organization, (2) data preprocessing, (3) development of a fault detection or prediction model, and (4) deployment and integration [16]. In this study, we focus primarily on step (3), which practitioners often divide into two sub-tasks: (i) the design of condition indicators and (ii) model training for fault detection or prediction tasks. The design of condition indicators (CIs) encompasses the computation and selection of features that correlate with the state of health of the system. A health indicator (HI) combines multiple condition indicators into a single efficient indicator that is highly informative of degradation [16, 25]. The separation of sub-tasks (i) and (ii) is instrumental in tackling the complexity of the problem, but often leads to suboptimality or extensive iterative improvements. We will address this concern in our contribution by means of multi-objective optimization methods that can inform the HI design, factoring in its prognostic efficacy.

For bearings, degradation is irreversible. Tracking the degradation state throughout the component's operational life can be effectively achieved with suitable sensors and signal processing techniques. The most prevalent failure mechanism under nominal conditions (where bearings are correctly installed and lubricated) is subsurface-originated spalling, which can be detected at an early stage using acoustic emission sensors[10]. Oil analysis sensors are highly effective for early detection of degradation in bearings and gearboxes,

#### 9:4 Spectral Fault Receptive Fields

as they quantify the accumulation of debris from the onset of wear processes [9]. While primarily limited to surface-related defects, the use of MEMS-based accelerometer sensors in our application domain enables cost-effective health monitoring solutions. Consequently, there is strong research interest in developing representations and algorithms capable of capturing early degradation and detecting incipient faults. Accelerometers are the standard transducers for helicopter gearbox condition monitoring, providing essential input to health and usage monitoring (HUM) systems. A healthy transmission exhibits a characteristic fingerprint, referred to as the regular meshing components of the signal [30]. For rolling bearings, the characteristic frequencies of their components are well established [29, 32], and their computation is readily available in standard predictive maintenance solutions [15]. Our work leverages this domain knowledge by explicitly computing representations that focus on the characteristic frequencies of bearing elements, aligning with established practices in vibration analysis and intelligent fault diagnosis for rotating machinery.

Faults can be classified based on their severity into three main categories: (1) abrupt, also known as stepwise fault; (2) incipient, also known as drifting; and (3) intermittent [26]. Incipient faults in bearings have weak signal signatures that are difficult to detect due to their stochastic nature, multiple transmission paths, and the aleatoric uncertainty present in mechanical systems [11]. Because of this, despite their well-understood spectral signatures, incipient fault detection remains an active area of research. Vibration signal analysis and modeling typically utilize degradation models that define at least two primary stages: (1) a flat, horizontal region corresponding to the healthy state, where remaining useful life (RUL) prediction is generally unreliable and arguably unnecessary, and (2) a degraded unhealthy state, which is the main focus of most analytical techniques for delivering accurate RUL estimates [13]. Piecewise linear models are often used to model this change in degradation dynamics [28]. Current research in bearing condition monitoring and prognosis is increasingly focused on extending the prediction horizon to encompass as much of the component's operational life as possible. In our present paper, we devise biologically inspired condition indicators that address the characterization of early degradation stages and not only correlate with manifested abrupt abnormalities.

There is a wide availability of vibration-based condition indicators in the literature. A taxonomy by Yan et al. [37] classifies them according to the representation domain: (1) time domain, (2) frequency domain, (3) time-frequency, and (4) wavelet. While this classification is not exhaustive, excluding some nonlinear feature extraction methods such as chaos-theoretic-based [11] and information-theoretic-based [32, 2], it nevertheless effectively represents the dominant approaches in the field. Among the most widely adopted characterizations are two statistical properties that can be computed regardless of the representational domain: (1) kurtosis-based, often spectral, and (2) RMS-based (with safety and vibration severity assessed by this metric, as in ISO 10816 [12]). Both are effective and can be used complementarily for different stages of the degradation process [6], while proven effective across diagnostic [23], condition monitoring [21], or prognostic [20] tasks. Our contribution builds on the frequency spectrum of vibration signals and is specifically designed for a low computational footprint, ensuring that it does not add significantly to the computational cost of the fast Fourier transform (FFT).

Our primary objective in this work is to engineer *health perception* systems capable of actively tracking the degradation state of bearings in alignment with defined cost and reliability constraints, thereby enabling accurate estimation of RUL. We adopt the term perception to underscore the biological inspiration behind our approach to CI construction. In biological systems, effective perception, of both the self and the environment, is essential

to survival: proprioception, homeostatic regulation [1], and autonomic functions support internal integrity and health, while environmental perception enables adaptive responses. Our approach subscribes to the principles of autopoiesis [17] and biological autonomy [22], where integrity is understood as an emergent property of systemic organization and constraint equilibria. This aligns well with closed-loop lifetime and degradation control algorithms [7].

To guide the construction of CIs, we draw inspiration from the biology of vision, specifically, the theory of center-surround opponency in the trichromatic visual system of primates, and adopt an adapted version of the difference-of-Gaussians (DoG) model, widely applied in both biological and artificial vision domains [33]. Derived from a novel transfer of computational models, we faced in our work the problem of appropriate parameterization of our Difference of Gaussians (DoG) method. Selecting the spectro-spatial scales relevant to bearing faults was achieved by relying on engineering judgement informed by field experience, a process we refer to as empirical parameter selection. We provide evidence that a DoG configured with these empirically chosen parameters encodes CIs effectively. To refine the model further for predictive-maintenance and prognostics applications, we optimised its parameters with a multiobjective genetic algorithm [4] guided by established condition-monitoring and prognosis criteria. Criteria must be quantifiable and provide foundations for certification [31]. Our results reveal a tradeoff, present among local Pareto-optimal front members, between the monotonicity criterion, widely advocated for health indicators [6, 27, 3, 8], and the accuracy of remaining-useful-life (RUL) predictions measured via normalised mean-squared error (MSE). Related work by Qin et al. [27] employs genetic programming to evolve an arithmetic condition indicator optimised for monotonicity within a Wiener stochastic framework that is subsequently refined through expectation-maximisation.

#### 3 Problem Domain and Dataset

### 3.1 XJTU-SY Bearing dataset

The experimental evaluation uses the XJTU-SY[36] run-to-failure bearing dataset, consisting of three bearing groups operated at fixed speeds and loads. Vibration signals were recorded with acceleration sensors along horizontal and vertical axes. Key bearing parameters include: inner raceway diameter ( $D_I = 29.30 \text{ mm}$ ), outer raceway diameter ( $D_O = 39.80 \text{ mm}$ ), pitch diameter ( $D_P = 34.55 \text{ mm}$ ), ball diameter ( $D_B = 7.92 \text{ mm}$ ), and contact angle ( $\phi = 0^{\circ}$ ), as illustrated in Figure 1. Bearings are uniquely labeled (e.g., "Bearing1\_1"), with data organized into snapshots (vibration signal temporal windows) taken at regular intervals.

### 3.2 Vibration Signatures of Bearings

We are interested in monitoring the degradation of the different elements of a bearing to detect incipient faults. Surface defects in these elements produce well-understood vibration signatures at characteristic frequencies, determined by the bearing's geometry and operational speed. Vibration signature analysis fundamentally depends on monitoring changes in vibration near the characteristic frequencies of bearings. As degradation progresses, the activity within these frequency bands evolves, reflecting the bearing's health state. Building on this established principle, our processing pipeline begins by computing these characteristic bands. While increased excitation in these bands is a hallmark of bearing defects, such activity can also be present throughout the bearing's operational life. For clarity and brevity, we refer to these as fault frequency bands, though their activity is not exclusively associated with faulty conditions, as some excitation is present throughout the bearing's operational life. Figure 2 shows the default sidebands obtained by MATLAB.

**Table 1** Characteristic frequencies related to bearing faults. BPFO = Ball Pass Frequency Outer Race; BPFI = Ball Pass Frequency Inner Race; BSF = Ball Spin Frequency; FTF = Fundamental Train Frequency (Cage).  $N_B$ : number of rolling elements;  $D_B$ : ball diameter;  $D_p = \frac{D_I + D_O}{2}$ : pitch diameter;  $\phi$ : contact angle;  $f_r$ : shaft rotational frequency.

Acronym	Equation
BPFO	$f_{\rm BPFO} = f_r \frac{N_B}{2} \left[ 1 - \frac{D_B}{D_P} \cos \phi \right]$
BPFI	$f_{\text{BPFI}} = f_r \frac{N_B}{2} \left[ 1 + \frac{D_B}{D_P} \cos \phi \right]$
BSF	$f_{\rm BSF} = f_r \frac{D_P}{2D_B} \left[ 1 - \left( \frac{D_B}{D_P} \cos \phi \right)^2 \right]$
FTF	$f_{\text{FTF}} = \frac{f_r}{2} \left[ 1 - \frac{D_B}{D_P} \cos \phi \right]$

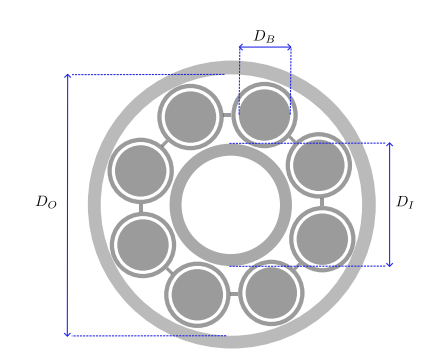


Figure 1 Schematic diagram of bearing geometry and parameters.

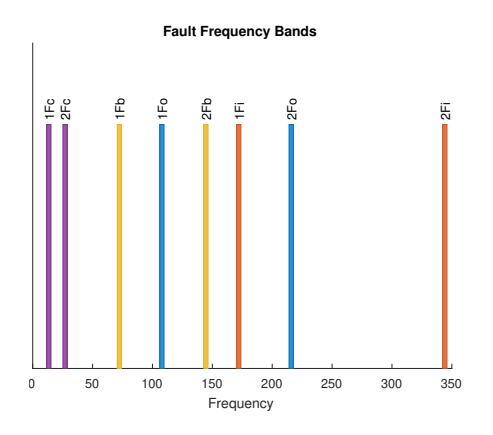
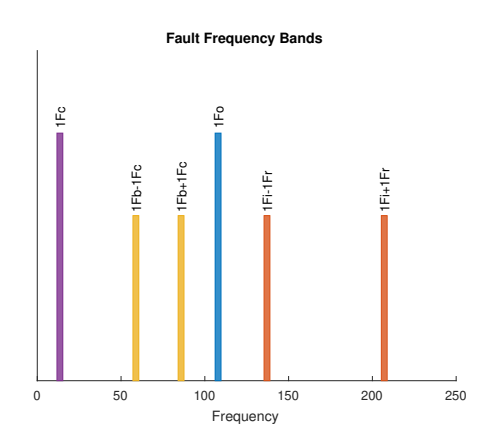


Figure 2 Fault Frequency Bands for the first and second harmonics. Notation: nF: the n-th harmonic for frequency F,  $F \in \{\text{Fo, Fi, Fc, Fb}\}$ . Frequencies are Fo: BPFO ( $f_{\text{BPFO}} = 107.9074$ ), Fi: BPFI ( $f_{\text{BPFI}} = 172.0926$ ), Fc: FTF ( $f_{\text{FTF}} = 13.4884Hz$ ), and Fb: BSF ( $f_{\text{BSF}} = 72.3300$ ).



**Figure 3** Fault Frequency Sidebands. Notation: nFb-mFc: the m-th negative sideband of n-th (central) harmonic frequency of Fb (nFb-mFc is obtained as  $n \times F_b - m \times F_c$ ), nFb+mFc: the m-th positive sideband of n-th (central) harmonic frequency of Fb (obtained with the sum).

For inner race defects, the fault interacts with the shaft's rotational speed because load distribution changes during each rotation, causing amplitude modulation. In this modulation, the characteristic inner race fault frequency acts as the carrier, while the shaft rotational frequency serves as the modulating signal. Similarly, amplitude modulation occurs between the ball spin frequency (BSF) and the fundamental train frequency (FTF), with the BSF as the carrier. This arises as the ball moves in and out of the load zone during cage rotation. Figure 3 illustrates the first-order sidebands associated with these phenomena.

# 4 Spectral Fault Receptive Fields

For each one of the faults, we will construct fault detectors inspired by the primate retinal ganglion cell receptive fields. Receptive fields in the primate retina are specific regions of the visual field where the presence of a stimulus (such as light or its absence) can excite (or inhibit) the activity of a ganglion cell. Although the retina encodes visual information

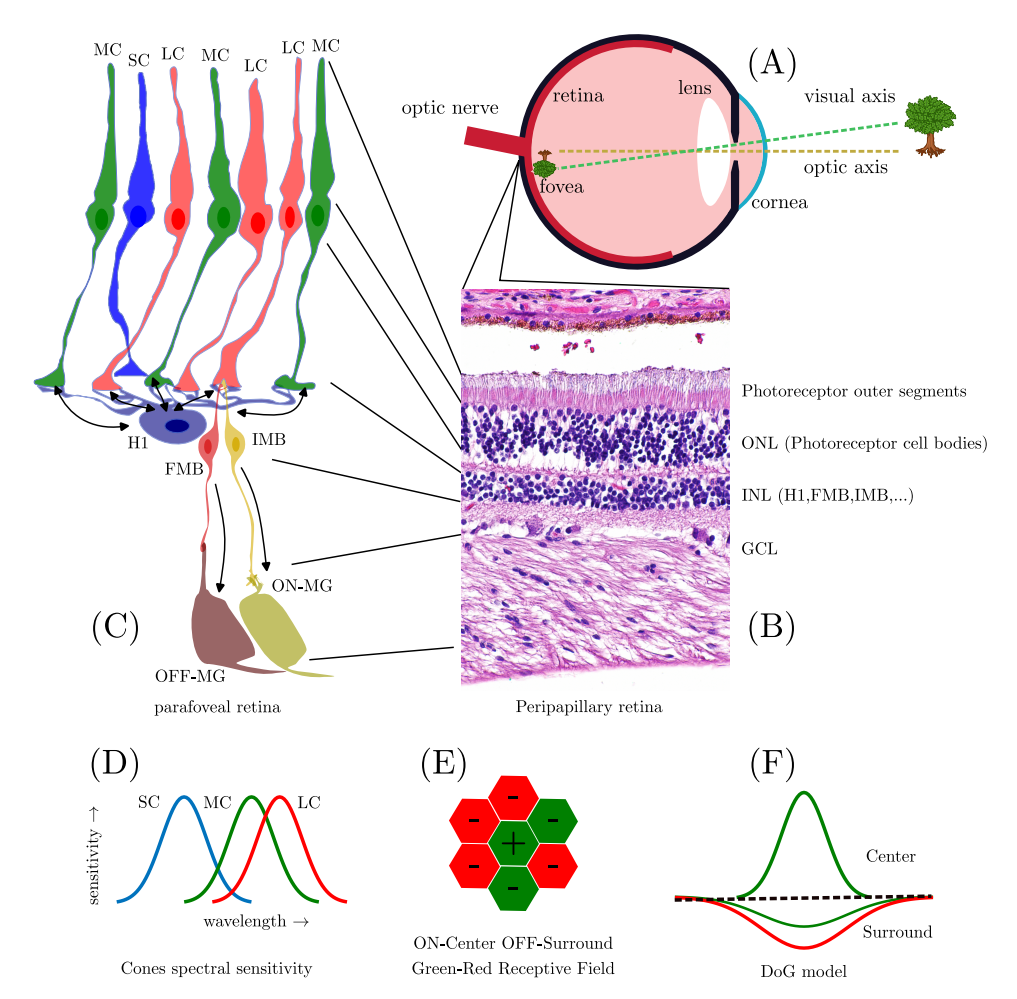


Figure 4 Encoding pathway underlying receptive field formation in primate retinal midget (P) ganglion cells. Insets: (A) eye anatomy highlighting retina, fovea, and image formation; (B) micrograph of peri-papillary retina layers (modified from [14]); (C) ON- and OFF-MG network in parafovea showing LC and MC cone synapses, H1 horizontal cells, flat and invaginating midget bipolar cells; (D) spectral sensitivity of cone types; (E) foveal cone mosaic depicting green-center red-surround receptive field; (F) DoG model illustrating center-surround color contrast.

through many parallel channels (processing chromatic, spatial, and temporal information), many image-forming retinal ganglion cells share a fundamental property: a center-surround spatial and chromatic organization. This type of processing encodes information about spatial and, for some cells, also chromatic contrast or differential excitation within the receptive field's spatial extent. Figure 4 illustrates the mechanisms of biological receptive fields inspiring our design of fault detectors that mimic center-surround contrast processing.

#### 4.1 Frequency Masks

To define the fault detectors, we utilize the frequency bands described in Section 3.2. Inspired by the center-surround organization of ganglion cell receptive fields, we introduce two distinct spectral extents, that is, frequency bands, with a narrower band representing the center and a broader band representing the surround. We implement the receptive fields in the frequency domain. Operating in this domain allows us to use a Gaussian function as the gain profile, which we call a spectral mask; this can be interpreted as implicit bandpass filtering.

**Table 2** Characteristic frequencies for bearing faults including harmonics and sidebands. Notation  $N_h$ : number of harmonics, and  $N_s$ : number of sidebands.

Fault Mode	Characteristic Frequencies
Outer race	$\mathcal{F}_O = \{ n f_{\mathrm{BPFO}} \mid n = 1N_h \}$
Inner race	$\mathcal{F}_{I} = \{ nf_{\text{BPFI}} + sf_{r} \mid n = 1N_{h}, \ s = -N_{s}N_{s} \}$
Ball	$\mathcal{F}_B = \{ n f_{\text{BSF}} + s f_{\text{FTF}} \mid n = 1N_h, \ s = -N_sN_s \}$
Cage	$\mathcal{F}_C = \{nf_{ ext{FTF}} \mid n = 1N_h\}$

The set  $\mathcal{M}$  of admissible spectral masks is defined as  $\mathcal{M} = \{m : \mathbb{R}_0^+ \to [0,1]\}$ . We restrict the domain to the non-negative real numbers because the spectral masks will act as a gain that will be multiplied by the absolute magnitude of the frequency components. Let  $M \subset \mathcal{M}$  be a finite subset of masks. We define the disjunction over M as the pointwise maximum over magnitudes as:

$$\bigvee M \in \mathcal{M}$$
, specifically,  $\bigvee M(f) = \max_{m \in M} m(f)$ .

Given the frequency band  $B = [f_{\min}, f_{\max}]$ , and the parameter  $k_{\sigma}$ , the Gaussian frequency mask G(f) is defined as:

$$G(f; B, k_{\sigma}) = \exp\left(-\frac{1}{2} \left(\frac{f - f_c(B)}{\sigma_f}\right)^2\right) \tag{1}$$

with  $f_c(B) = \frac{f_{\min} + f_{\max}}{2}$ , and  $\sigma_f = \frac{f_{\max} - f_{\min}}{2 \cdot k_{\sigma}}$ . The parameter  $k_{\sigma}$ , called the sigma rule, determines how the limits of the frequency bands are handled. A sigma rule of 3 corresponds to 99.7% of the area under the Gaussian falling within the specified frequency band.

### 4.2 SFRFs Computation

An advantage of filtering in the frequency domain is that it enables all operations to be computed simultaneously by precomputing a single gain mask across the spectrum for each operational mode. This strategy is particularly efficient because, although the characteristic frequencies of interest shift with the shaft speed, the frequency-domain filters can be generated in advance, and applying the filter is equivalent to a Hadamard product (elementwise multiplication) between the spectrum of the vibration signals and the mask corresponding to the appropriate operational mode.

The characteristic frequencies for each fault mode are defined as shown in Table 2. We define the corresponding frequency bands as  $\mathcal{B}(F,W) = \{[f - \frac{W}{2}, f + \frac{W}{2}] \mid f \in F\}$ . Given the set the characteristic frequencies  $\mathcal{F} \in \{\mathcal{F}_O, \mathcal{F}_I, \mathcal{F}_B, \mathcal{F}_C\}$ , and shape parameters  $\sigma_C = (\mathcal{W}_C, \kappa_C)$  for the center and  $\sigma_S = (\mathcal{W}_S, \kappa_S)$  for the surround. Then given  $\sigma = (\mathcal{W}, \kappa) \in \{\sigma_C, \sigma_S\}$  we can define a receptive field gain function as:

$$\mathcal{G}^{\sigma}_{\mathcal{F}} \in \mathcal{M}, \quad \text{specifically,} \quad \mathcal{G}^{\sigma}_{\mathcal{F}} = \bigvee \left\{ G(f; B, \kappa) : B \in \mathcal{B}(\mathcal{F}, \mathcal{W}) \right\}.$$

We refer to  $W_{\mathcal{C}}$  as the center bandwidth and  $W_{\mathcal{S}}$  as the surround bandwidth. The *Difference of Gaussians* used to compute the SFRF is then given by:

$$DoG = \int_{0}^{\frac{f_{S}}{2}} \left[ \mathcal{G}_{\mathcal{F}}^{\sigma_{C}}(f) - \kappa_{H} \, \mathcal{G}_{\mathcal{F}}^{\sigma_{S}}(f) \right] |A(f)| \, df \tag{2}$$

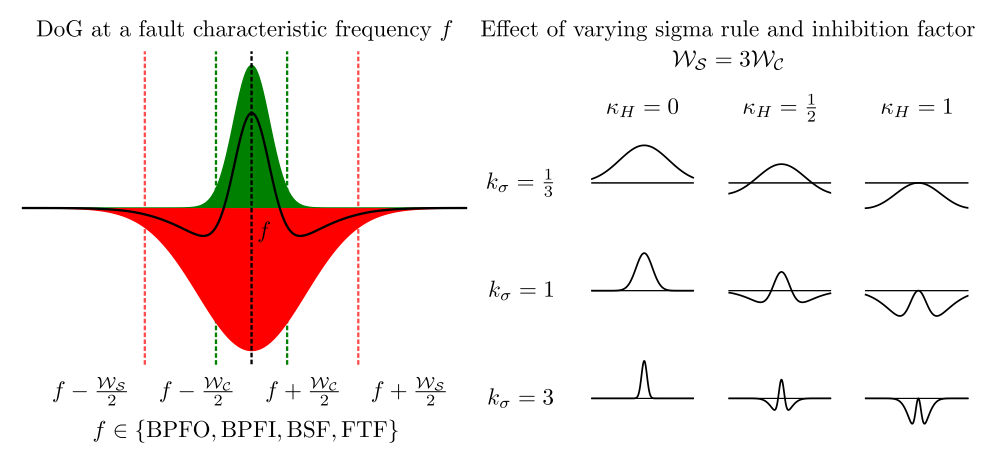
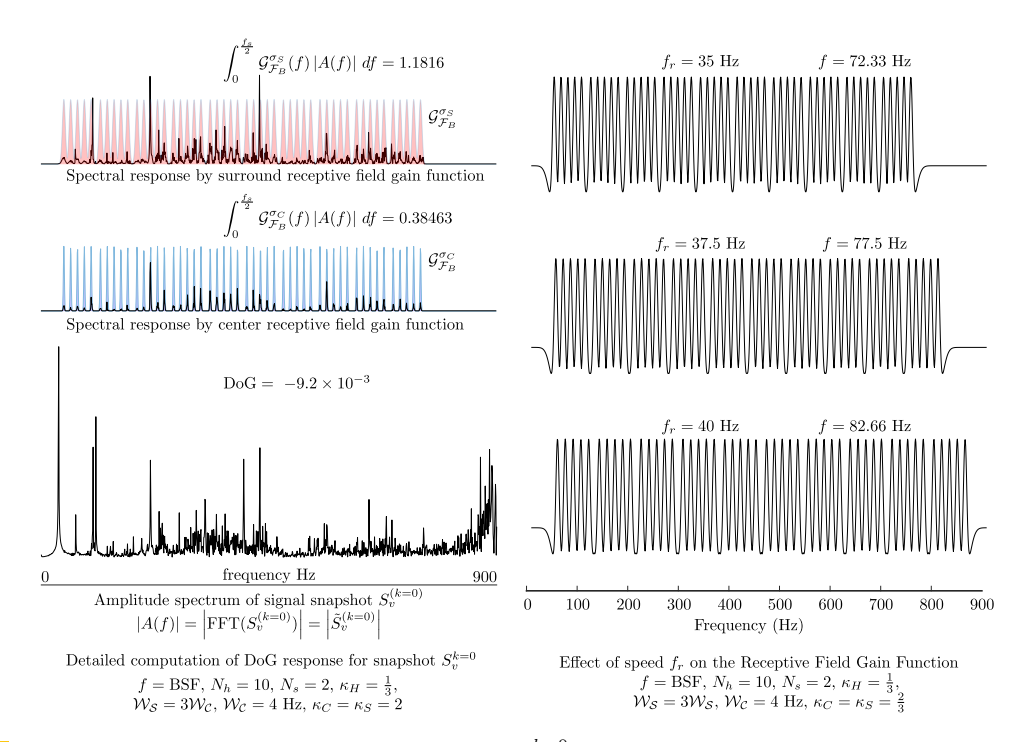


Figure 5 Parameters of the Difference of Gaussians (DoG) model. Left: Illustration of a DoG model centered at a fault characteristic frequency. For the receptive field gain functions  $\mathcal{G}_{\mathcal{F}}^{\sigma}$ , these are defined for the applicable harmonics and sidebands (see Tables 1 and 2). Right: Effect of varying the sigma rule  $k_{\sigma}$  ( $k_{\sigma} = \kappa_{C} = \kappa_{S}$ ) and the inhibition factor  $\kappa_{H}$  under the condition  $\mathcal{W}_{S} = 3\mathcal{W}_{C}$ .



**Figure 6** Computation of DoG for snapshot  $S_v^{k=0}$  and fault type Ball, and effect of speed on receptive field gain function (RFGF). Left, bottom to top: unfiltered amplitude spectrum, spectrum filtered by center RFGF  $\mathcal{G}_{\mathcal{F}}^{\sigma_C}$ , and spectrum filtered by surround RFGF  $\mathcal{G}_{\mathcal{F}}^{\sigma_S}$ . Numeric integrals and final DoG computation included. Right: Effect of shaft speed  $f_r$  on DoG RFGF,  $\mathcal{G}_{\mathcal{F}}^{\sigma_C} - \kappa_H \mathcal{G}_{\mathcal{F}}^{\sigma_S}$ .

where f denotes frequency in the vibration spectrum,  $f_s$  the sampling frequency, and  $A(f) = \tilde{S}^{(k)}(f)$  is the Fourier transform of the  $k^{\text{th}}$  accelerometer signal snapshot  $S^{(k)}$ . The parameters  $\kappa_C$  and  $\kappa_S$  control the width (sigma rule) of the center and surround Gaussians, respectively, and  $\kappa_H$  is the inhibition factor. Figure 5 illustrates these parameters and their effect in the shape of the gain profiles. Figure 6 illustrates the DoG computation and the adaptation of the receptive field gain functions with shaft speed. Figure 7 depicts the processing pipeline and detail SFRFs computation.

# 5 Experimental Evaluation

In this section, we evaluate the suitability of SFRFs for condition monitoring. Traditionally, condition monitoring relies heavily on identifying condition indicators and health indices that effectively capture the degradation trend of a system. This effectiveness is often assessed using metrics such as monotonicity, prognosability, and trendability. However, the XJTU-SY dataset contains only five samples per operational condition, which is insufficient for meaningful analysis of prognosability and trendability, since these metrics require larger datasets. Therefore, we selected monotonicity as the primary evaluation criterion. This choice is justified because, if a signal is to reliably capture degradation and we assume no regenerative processes, as is typical in the mechanical system under study, there must be a consistent correlation between the values of the condition indicators or health index and the operational time of the machine. However, it is important to note that expecting perfect monotonicity is unrealistic. Aleatoric uncertainties, unknown inputs, and varying environmental contexts naturally introduce fluctuations into the estimations. For this reason, we also consider the smoothness of the condition indicator as an additional evaluation metric.

### 5.1 Empirical Selection of Parameters

We report the qualitative behavior of condition indicators  $C^{(k)}$  obtained using SFRFs for different fault types on the bearing labeled  $Bearing1\_1$ . Since SFRF is a novel technique with many unknowns, we first present results based on empirical choices.

Inspired by the qualitative behavior of receptive fields of primate parvocellular ganglion cells, we chose a center contribution stronger and narrower than the surround. Two parameter sets control the frequency span: bandwidths  $W_C$ ,  $W_S$ , and frequency attenuation sharpness given by sigma rules  $\kappa_C$  and  $\kappa_S$ . Bandwidth selection focused on limiting spatial overlap among fault bands while capturing natural frequency deviations near characteristic fault frequencies within the constraints of the dataset's maximum frequency resolution (0.78125 Hz). We adopt a center-to-surround bandwidth ratio of 1:3, with  $W_C = 4$  Hz and  $W_S = 12$  Hz. The sigma parameters are set as  $\kappa_C = \kappa_S = 2$ . For the DoG computation,  $N_h = 10$  harmonics and  $N_s = 2$  sidebands are used, with inhibition factor  $\kappa_H = \frac{1}{3}$ .

#### 5.2 Evaluation of SFRF with Empirical Parameters

We computed the SFRFs response to horizontal and vertical acceleration and visualized the temporal behavior of the SFRFs to assess whether they can capture the degradation trend of the bearing. Figure 8 shows the temporal behavior of the four SFRFs. It can be observed that all SFRFs are capable of detecting a sudden transition in the temporal evolution. This behavior is reasonably interpreted as the manifestation of a defect, with the degradation trajectories for the inner and outer race SFRFs differing significantly around time 80.

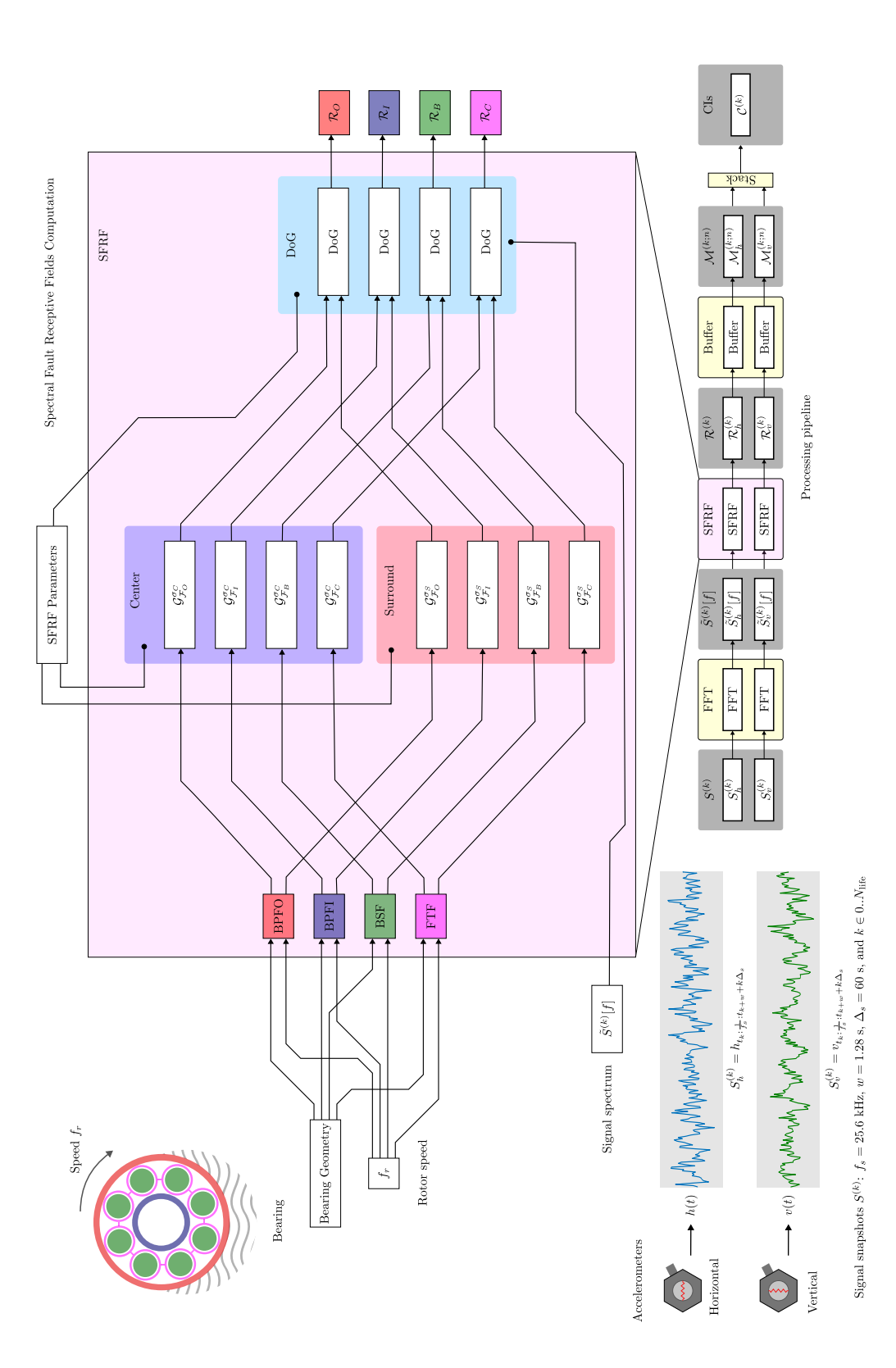


**Figure 7** Computation of SFRFs and processing pipeline. Bottom left: vibration signals from two accelerometers; snapshots indexed by k. Bottom right: pipeline computes FFT and SFRFs per channel, stores computed vectors in a buffer, and stacks channels to form CIs. Top: exploded view of SFRF computation using shaft speed, vibration spectrum, bearing geometry, and SFRF parameters.

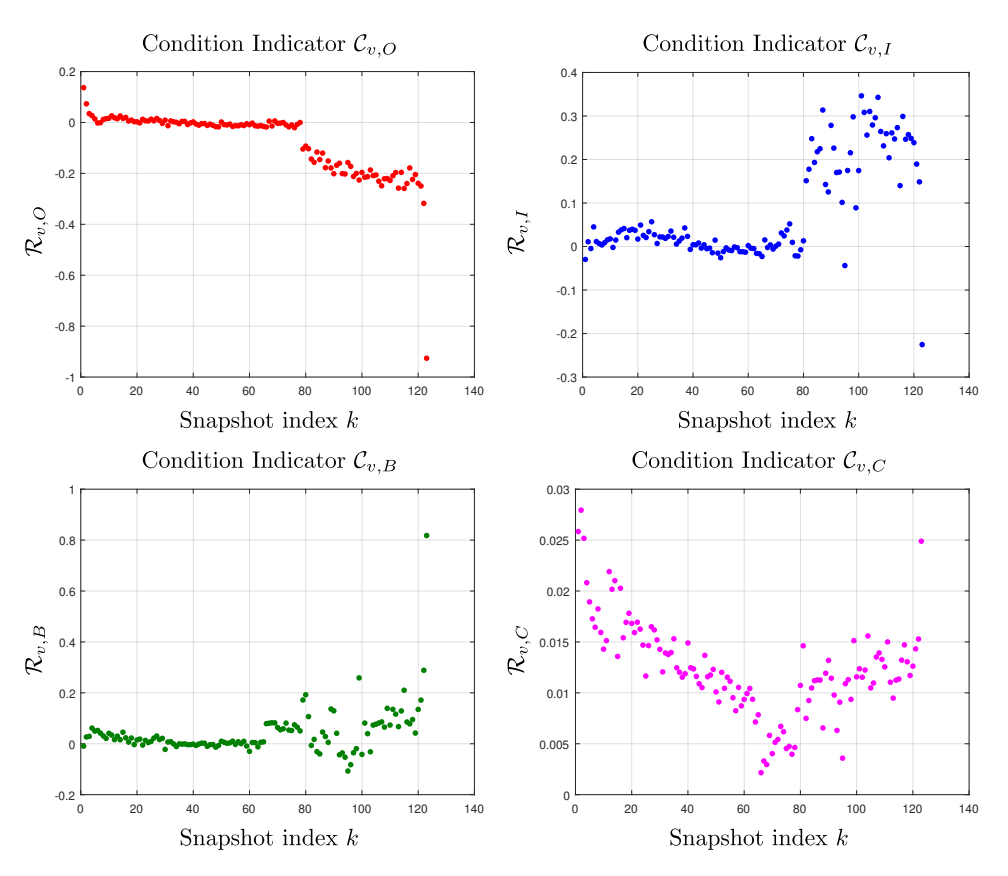


Figure 8 Temporal behavior of condition indicators for the four fault types and vertical vibrations of bearing Bearing 1\_1, under operating conditions of shaft speed  $f_r = 35$  Hz and load 12 kN.

Another observation from the ball CI  $C_{v,B}$  in Figure 8 is its early response to an event, around time 65, before outer  $(C_{v,O})$  and inner race  $(C_{v,I})$  CIs exhibit any noticeable change. This behavior may reasonably be interpreted as indicating either the onset of a less severe defect or a precursor to the severe fault, detected at about time 80 by all CIs. Notably, this abrupt change in the degradation trajectory is also perceived by the cage CI  $(C_{v,C})$ . The cage CI, in particular, captures the early degradation pattern effectively, displaying a consistent trend from the beginning up to the early event. This suggests that, even with a crude heuristic parameter selection, the combination of cage and ball CIs may offer a reliable monitoring of degradation since the very beginning of the operational life of the bearing.

### 5.3 Optimizing for Condition Monitoring and Prognosis

Our qualitative results are encouraging but also highlight several issues with the current method, the most notable being the varying sensitivity of different CIs to degradation events. Evolutionary multi-objective optimization techniques are particularly well-suited for scenarios where theoretical guidance is limited, as they require minimal assumptions and can efficiently explore complex parameter spaces. In this context, we formulated the exploration of the SFRFs parameter space as an optimization problem, explicitly quantifying our condition monitoring and prognosis criteria and defining them as objectives to be optimized. Table 3 presents these three objectives. The first objective directly assesses the model's predictive accuracy by quantifying the error in remaining useful life (RUL) estimation. The second objective encourages consistent sensitivity to degradation across the component's lifetime.

**Table 3** Optimization objectives for NSGA-II. Notation: CIs are concatenated into a time-varying condition indicator vector  $x^{(t)}$  (subsampled from  $\mathcal{C}^{(k)}$ ) of dimension F (4 CIs from  $\mathcal{C}^{(k)}_h$ ) and 4 CIs from  $\mathcal{C}^{(k)}_v$ ),  $\rho_j$  is the Spearman correlation between feature j and snapshot time, and  $\Delta x^{(t)}_j$  is the first difference of the j-th SFRFs at time t,  $y^{(t)}$  is the observed RUL at time t while  $\hat{y}^{(t)}$  the predicted RUL, both quantities are normalized by the maximum RUL.

$$\begin{array}{ll} \text{Objective} & \text{Equation} \\ \text{RUL Error (MSE)} & \frac{1}{K} \sum_{i=1}^{K} (y^{(t)} - \hat{y}^{(t)})^2 \\ \text{Monotonicity} & \left(\prod_{j=1}^{F} |\rho_j|\right)^{1/F} \\ \text{Smoothness (MAD)} & \left(\prod_{j=1}^{F} \operatorname{median} \left(\left|\Delta x_j^{(t)} - \operatorname{median} \left(\Delta x_j^{(t')}\right)\right|\right)\right)^{1/F} \end{array}$$

The third objective penalizes jitter along the degradation trajectory, thereby promoting smoother and more interpretable trends. We chose to use the geometric mean rather than conventional averaging to ensure that no individual CI is overlooked during the optimization process. Although it is theoretically possible to avoid aggregating the behaviors altogether and instead treat each CI as an independent objective, this alternative was not pursued in the present study. In retrospect, formulating the optimization of different SFRFs as independent optimization problems may represent a better path, since their computations do not depend on one another. We leave this possibility open for exploration in future work.

A key advantage of surrogate models lies in the efficient computation of objectives, which is essential given the population-based nature of evolutionary algorithms, where a single run may involve thousands of evaluations. To predict the RUL, we trained a bagging regression ensemble model on a sub-sampled degradation trajectory of Bearing1\_1. This strategy offers several benefits: (1) bagging regressors, as ensemble methods, provide robust predictions with a reduced risk of overfitting; (2) they perform well even with limited data; and (3) they are computationally efficient, making them well-suited as surrogate models during optimization.

However, this decision also introduces a notable challenge: bagging regressors are inherently nondeterministic, which can lead to fluctuations in the Pareto front during optimization. We consider this acceptable, even somewhat beneficial, as the stochasticity helps mitigate overfitting and discourages convergence toward non-robust regions of the parameter space, which is particularly important when working with limited data.

We performed the optimization of SFRFs parameters with MATLAB's gamultiobj function using the algorithm's default settings and the following domain bounds for the parameters:  $\kappa_C, \kappa_S \in [n^{-2}, n^2] \kappa_H \in [0, 1]$  with n = 3. Figure 9 presents the local Pareto-optimal front after 155 iterations, at which point the convergence criterion was satisfied (i.e., the change in the spread of Pareto solutions is less than  $1 \times 10^{-4}$ ). NSGA-II identifies a diverse set of non-dominated solutions. As the optimization function performs minimization in all objectives, we changed the sign of monotonicity and smoothness to enforce their maximization.

Several findings are noteworthy. First, all Pareto-optimal individuals cluster within a region where the sigma rule center spreads up to a maximum of 6, while the sigma rule surround spreads up to a maximum of 2. This aligns with our expectation that the surround performs better when covering a wider frequency bandwidth (the higher the sigma rule, the stricter the Gaussian). However, it is somewhat surprising that this was not already enforced by setting the surround bandwidth  $W_S$  to be three times that of the center  $W_C$ .

We observe that most objectives conflict with each other. The algorithm's selection mechanism, which emphasizes boundary individuals through its use of crowding distance, tends to favor solutions at the extremes of the objective space in order to maximize diversity across the Pareto front. Despite leveraging interactive visualizations, we did not identify the

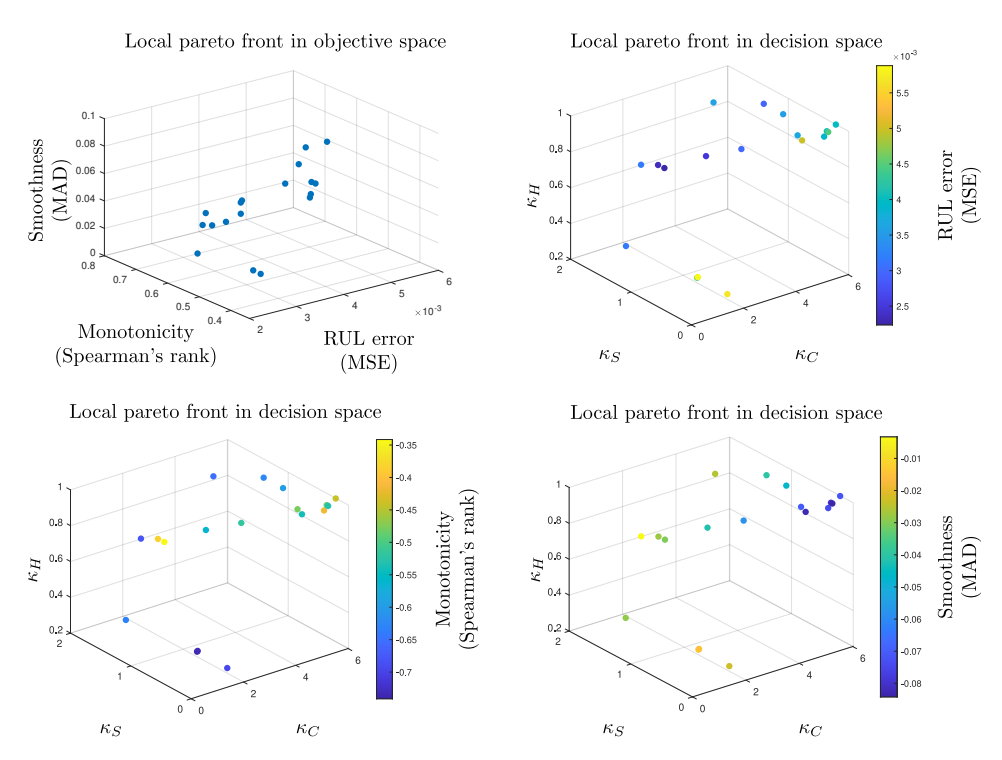


**Figure 9** The local Pareto-optimal front identified by NSGA-II after 155 iterations and 7,750 function evaluations. Top left panel visualizes individuals in the objective space. The remaining panels depict the parameter space, with solution colors encoding different objectives (in the color bars, the sign of monotonicity and smoothness is reversed, deep blue colored solutions are better).

anticipated cooperation between monotonicity and RUL prediction accuracy. Specifically, solutions exhibiting high monotonicity (deep blue in the monotonicity inset) often perform poorly in terms of RUL prediction, and vice versa, those with low RUL error (deep blue in the RUL error domain) tend to score low in monotonicity.

This limitation is particularly evident in the case of our cage CI, which, despite being highly informative of degradation throughout the entire operational life, would be penalized by conventional monotonicity metrics. Its triangular shape, coupled with relatively low energy content and a noisy appearance, would result in a low monotonicity score. However, the fundamental issue extends beyond this specific example and lies in the distinction between local and global trends, as well as in the methodology used to compute monotonicity. Traditional condition indicators are computed episodically rather than as states of dynamical processes. In simple degradation models, the health condition is typically evaluated based on a single temporal snapshot, without consideration for the underlying trend or the temporal evolution of the indicator. This highlights the need for monotonicity metrics or health indicators that account for temporal dynamics on multiple temporal scales.

These findings suggest that CIs should be evaluated as dynamic processes, not merely as isolated episodes. This supports the adoption of stochastic differential equations as robust models for degradation processes. Moving forward, our future research should focus on stochastic model identification and the tracking of their parameters, which may provide a more nuanced and accurate assessment of system health and more rational RUL estimations.

We repeated our qualitative evaluation of the CIs, this time selecting the individual from the Pareto front that achieved the best RUL prediction performance. This individual is characterized by the following parameters:  $\kappa_C = 1.0253$ ,  $\kappa_S = 0.8905$ , and  $\kappa_H = 0.8647$ .

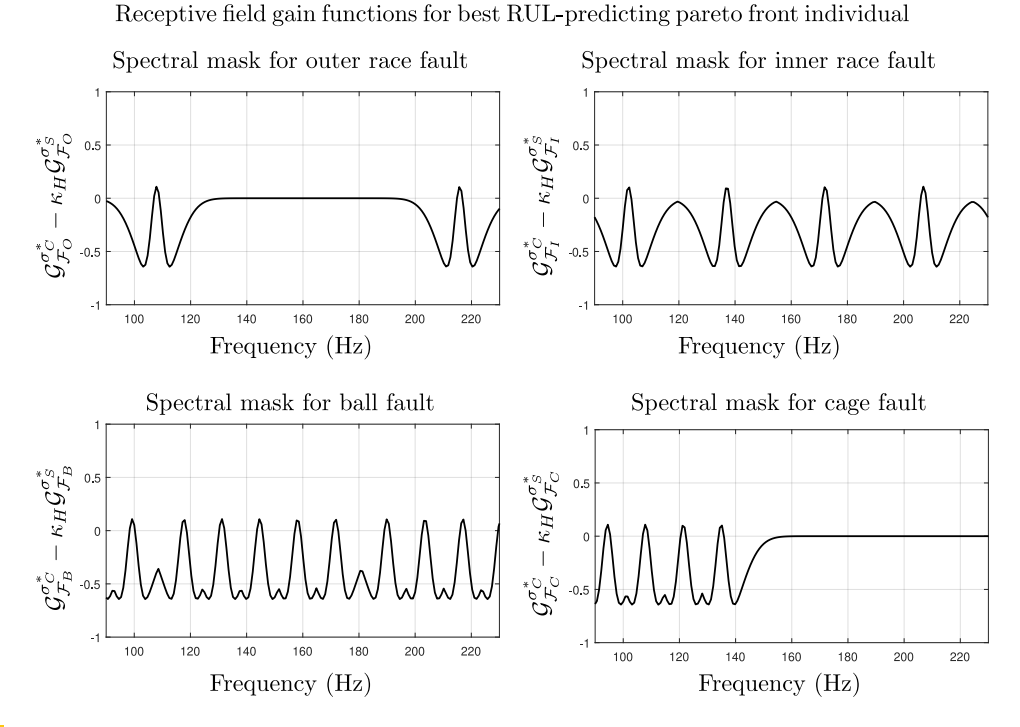


Figure 10 DoG RFGFs for the best RUL-predicting individual on the local Pareto-optimal front. Operating conditions: shaft speed  $f_r = 35$  Hz and load 12 kN. Only the 90-230 Hz band is shown.

Figure 10 illustrates the RFGFs corresponding to this optimal parameter set within the local Pareto-optimal front, as determined by the lowest RUL prediction error. The receptive fields exhibit an excitatory center but primarily operate within the inhibitory region. Notably, a cumulative effect, kept in check by the max operator, emerges when the Gaussian surrounds overlap, particularly for the ball and cage CIs (see bottom insets). This overlap causes the receptive fields to compute spectral contrast across the local spectrum. As we established broad parameter ranges for the genetic algorithm to explore candidate solutions, including configurations with weak or no inhibition, the observed convergence towards solutions with strong and wide inhibitory surrounds indicates a positive relationship between spectral contrast and the criteria for condition monitoring and prognosis. If traditional approaches relying solely on filtering characteristic frequencies were superior, the genetic algorithm would have favored those simpler solutions. Instead, it evolved more complex inhibitory surrounds essential for effective contrast computation, highlighting the importance of antagonistic spectral filtering in enhancing degradation state assessment.

Regarding the utility of SFRFs as CIs, Figure 11 presents a comparison between the empirically obtained CIs analyzed in the previous section and those corresponding to the most performant RUL prediction solution. The evolved CIs better characterize degradation trends and more clearly signal the onset of defects compared to their empirical counterparts. Notably, the ability of the cage CI to correlate with degradation from the beginning of the bearing's operational life is further enhanced by the evolutionary algorithm.

To test our hypothesis that RUL predictions should account for the temporal evolution of condition indicators, we conducted experiments in which we varied the order of the condition indicators used for prediction. Following standard dynamical systems terminology, we refer to the *zero-order* indicator as the instantaneous condition indicator (although it is

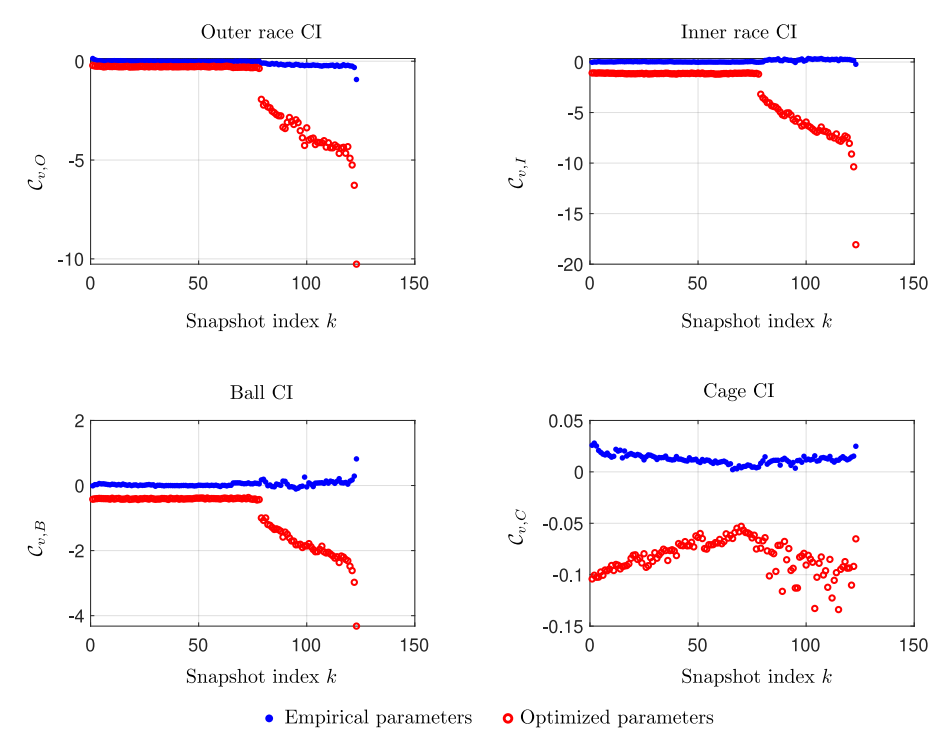


Figure 11 Comparison of CIs obtained with empirical parameters (blue filled circles) versus the best RUL-predicting local Pareto-optimal solution (open red circles).

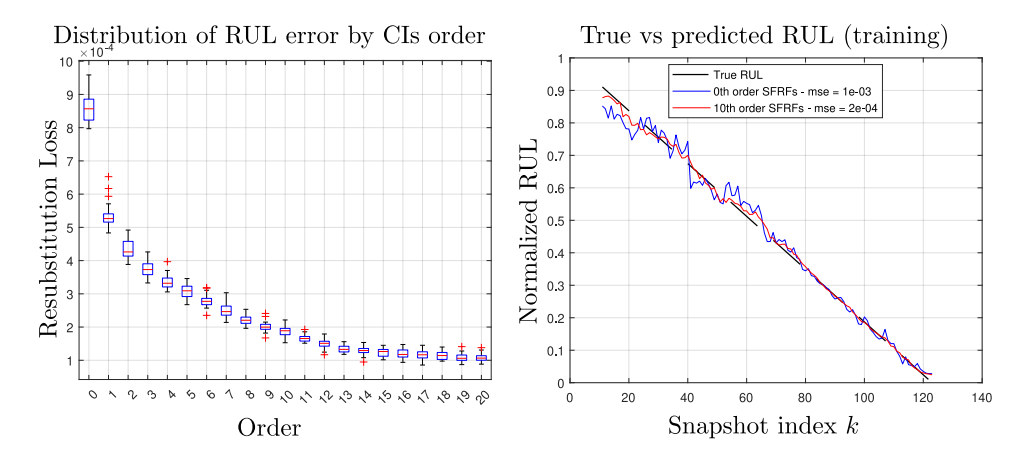
computed from a signal snapshot of 1.28 seconds) represented by the eight CIs (four fault types across two vibration signals). The *first-order* indicator is a 16-dimensional vector formed by concatenating the current CIs with those from the previous time step. More generally, the n-th order CI corresponds to an 8(n+1)-dimensional vector comprising the current CI and a buffer containing the previous n sets of CIs. This formulation allows the model to incorporate temporal context and memory into the RUL prediction process.

Figure 12 illustrates the effect of varying the SFRF order on prediction performance. The left inset shows the resubstitution loss of bagging regressor models trained with different orders. Due to the model's nondeterministic nature, we repeated the training 30 times and used box plots to represent the distribution of errors for each order. We observe that using a second-order SFRF condition indicator vector can reduce the resubstitution loss by approximately half. The right-hand visualization demonstrates the impact of SFRF order on RUL prediction accuracy; notably, the 10th-order predictor exhibits a marked improvement, closely tracking the true RUL across the entire operational life.

While these results are encouraging, they reflect only the *training* loss and must be substantiated through rigorous cross-validation methodologies. Nevertheless, the findings underscore the potential value of incorporating temporal memory into RUL estimation.

#### 6 Discussion

Drawing inspiration from the biology of vision, we have explored the implementation of SFRFs based on the characteristic frequencies of bearing elements, their harmonics, and known amplitude modulation phenomena. This leads to implicit spectral filters that adapt naturally to varying speed conditions (see Figure 6). SFRFs compute spectral activity contrast in a



**Figure 12** Training (resubstitution) MSE error with increasing orders and comparison of RUL estimations between 0th order and 10th order SFRFs.

manner analogous to how visual systems encode chromatic information. However, instead of excitation by light and preferential responses to different wavelengths by photopigments in cone photoreceptors, we analyze vibration signals transformed into the frequency domain. By monitoring the characteristic frequencies associated with different bearing components, SFRFs enable us to track degradation trends throughout the operational life of the machinery. Our particular implementation relies on the computation of Gaussian spectral filters centered at the characteristic frequencies, numerical integration of frequency bins across the spectrum, and the evaluation of spectral contrast, which depends on integrated energy within a narrow bandwidth we call the center, and a wider bandwidth, the surround. The DoG model, adapted to our domain, was formally defined and implemented. Its definition aims for computational efficiency. Our qualitative evaluation of the SFRFs for monitoring health state demonstrates their potential as effective condition indicators. The trends observed throughout the operational history indicate that SFRFs can detect abrupt defect events. Furthermore, they appear capable of capturing the gradual evolution of degradation. In addition, these findings support using SFRFs for fault detection and potentially diagnosis, as their outputs correspond to specific failure modes. However, a decision layer is essential to harmonize the degradation trends from different CIs. This integration is reserved for future research, as it requires further development and validation. Alternatively, the multi-objective algorithm could explicitly optimize diagnostic performance if suitable datasets are available.

Different SFRFs exhibit unique behaviors and require appropriate parameter tuning to maximize their effectiveness. Building on these insights, we established quantitative criteria to assess the suitability of various parameters in the Difference of Gaussians (DoG) model, ensuring the extraction of features that are relevant for condition monitoring and prognosis. We use a multiobjective genetic algorithm to compute an approximate Pareto-optimal set of solutions. To guide the optimization, we incorporated three objectives: first, the RUL prediction error, evaluated using fast surrogate RUL estimators instantiated as bagging regressor models; second, monotonicity, which is widely recognized in the PHM community as a crucial metric for feature selection in prognostic pipelines; and third, smoothness, which targets the desirable property of stability in condition monitoring indicators. We contrasted the quality of the best predictor against the empirical counterpart, demonstrating the value of the optimization stage. We also observed, through analysis of the cage CIs, that certain feature indicators may provide valuable information for condition monitoring and prognosis,

#### 9:18 Spectral Fault Receptive Fields

yet may be overlooked or rejected when evaluated solely by standard monotonicity metrics. This highlights the need for the development of more sophisticated evaluation criteria that can capture the full prognostic value of such features. Motivated by this observation, we investigated the impact of incorporating local temporal trends by stacking the CIs in a memory buffer. We assessed RUL predictions across different orders, and our results confirm that incorporating temporal context significantly reduces prediction error.

We acknowledge the preliminary nature of our contribution. Notably, the distinct spectrotemporal properties exhibited by different SFRFs suggest that their parameters should be tuned independently, as a one-size-fits-all approach may be overly simplistic. Drawing further inspiration from biology, it is well established that retinal ganglion cells operate in parallel channels, each capturing diverse spectro-spatio-temporal properties and contributing to a robust and flexible representation. Similarly, future research could explore the simultaneous deployment of a diversity of solutions along the Pareto front through ensemble techniques. By orchestrating and interpreting the responses of multiple SFRFs, it may be possible to achieve more comprehensive and adaptable representations, where individual SFRFs provide complementary, partial views tailored to specific objectives. For instance, some SFRFs may be better suited for condition monitoring, others for RUL prediction, and their relative importance or activity could adapt dynamically depending on the degradation state. Currently, FFT computation is the most resource-intensive step in the pipeline. However, next-generation sensors could be designed to shift the focus from general-purpose accelerometers to resonant arrays that respond preferentially to the engine's spectral fingerprint, potentially eliminating the need for FFT altogether.

# 7 Conclusions

This study demonstrates the value of drawing inspiration from nature to develop robust and reliable systems. Spectral fault receptive fields show considerable promise as foundational elements for condition monitoring and prognosis. They also have a minimal computational footprint, making them well-suited for onboard deployment in EVPs. Our qualitative evaluation indicates that, particularly in their optimized form, SFRFs are well-suited for both condition monitoring and remaining useful life (RUL) estimation.

We conclude that by integrating established vibrational analysis techniques with conceptual models from biological perception, and with the help of evolutionary algorithms, it is possible to devise effective solutions for tracking degradation states throughout the operational life of bearings. These types of biologically inspired solutions open new possibilities for advancing predictive maintenance and enhancing the reliability of industrial machinery.

# References

- Peter M. Asaro. From Mechanisms of Adaptation to Intelligence Amplifiers: The Philosophy of W. Ross Ashby. In Philip Husbands, Michael Wheeler, and Owen Holland, editors, *The Mechanical Mind in History*, pages 153–176. MIT Press, Cambridge, MA, 2008. doi: 10.7551/mitpress/7626.003.0008.
- Wahyu Caesarendra, Buyung Kosasih, Kiet Tieu, and Craig A.S. Moodie. An application of nonlinear feature extraction A case study for low speed slewing bearing condition monitoring and prognosis. In 2013 IEEE/ASME International Conference on Advanced Intelligent Mechatronics, pages 1713–1718, 2013. doi:10.1109/AIM.2013.6584344.
- 3 Xiao-Dan Chen, Ke Li, Shao-Fan Wang, and Hao-Bo Liu. Switching Unscented Kalman Filters With Unknown Transition Probabilities for Remaining Useful Life Prediction of Bearings. IEEE Sensors Journal, 24(20):32577–32595, 2024. doi:10.1109/JSEN.2024.3445934.

- 4 Kalyanmoy Deb, Amrit Pratap, Sameer Agarwal, and T. Meyarivan. A Fast and Elitist Multiobjective Genetic Algorithm: NSGA-II. *IEEE Transactions on Evolutionary Computation*, 6(2):182–197, 2002. doi:10.1109/4235.996017.
- 5 Department of Defense, Washington, DC. MIL-HDBK-217F: Military Handbook Reliability Prediction of Electronic Equipment, 1991. Superseding MIL-HDBK-217E, Notice 1, 2 January 1990.
- 6 S.J. Engel, B.J. Gilmartin, K. Bongort, and A. Hess. Prognostics, the real issues involved with predicting life remaining. In 2000 IEEE Aerospace Conference. Proceedings (Cat. No.00TH8484), volume 6, pages 457–469 vol.6, 2000. doi:10.1109/AERO.2000.877920.
- 7 Mônica S Felix, John J Martinez, and Christophe Bérenguer. Remaining Useful Life (RUL) Control of Controlled Systems under Degradation. *Authorea Preprints*, 2024. Submitted to International Journal of Robust and Nonlinear Control. doi:10.22541/au.172146328.87517875/v1.
- 8 Ying Fu, Ye Kwon Huh, and Kaibo Liu. Degradation Modeling and Prognostic Analysis Under Unknown Failure Modes. *IEEE Transactions on Automation Science and Engineering*, 22:11012–11025, 2025. doi:10.1109/TASE.2025.3530845.
- Gill Sensors & Controls. WearDetect explained (5 minute video), 2024. Accessed: 2025-06-10. URL: https://gillsc.com/weardetect-explained-5-minute-video/.
- Einar Løvli Hidle. Early Detection of Subsurface Cracks in Rolling Element Bearings using the Acoustic Emission Time Series. Master's thesis, Norwegian University of Science and Technology (NTNU), 2021. URL: https://ntnuopen.ntnu.no/ntnu-xmlui/handle/11250/2826382.
- Jinqiu Hu, Laibin Zhang, Wei Liang, and Zhaohui Wang. Incipient mechanical fault detection based on multifractal and MTS methods. *Petroleum Science*, 6(2):208–216, 2009. doi: 10.1007/s12182-009-0034-8.
- 12 International Organization for Standardization. ISO 20816-3:2022. Mechanical vibration Measurement and evaluation of machine vibration Part 3: Industrial machines with nominal power above 15 kW and nominal speeds between 120 r/min and 30 000 r/min, 2022.
- Yaguo Lei, Naipeng Li, Liang Guo, Ningbo Li, Tao Yan, and Jing Lin. Machinery health prognostics: A systematic review from data acquisition to RUL prediction. *Mechanical Systems and Signal Processing*, 104:799–834, 2018. doi:10.1016/j.ymssp.2017.11.016.
- Librepath. Micrograph showing optic nerve head and retina. H&E stain. https://commons.wikimedia.org/wiki/File:Retina\_--\_high\_mag.jpg, 2015. Creative Commons Attribution-Share Alike 3.0 Unported license (CC BY-SA 3.0).
- 15 MathWorks. Predictive Maintenance Toolbox User's Guide R2024b. MathWorks, 2018. URL: www.mathworks.com.
- MathWorks. Predictive Maintenance Toolbox Getting Started Guide. MathWorks, 2024. Release R2024b, originally published 2018. URL: https://www.mathworks.com/help/predmaint/index.html
- 17 Humberto R. Maturana and Francisco J. Varela. De máquinas y seres vivos: Autopoiesis: La organización de lo vivo. Editorial Universitaria. LUMEN., Santiago, Chile, 1972.
- James G. McLeish. Enhancing MIL-HDBK-217 reliability predictions with physics of failure methods. In 2010 Proceedings - Annual Reliability and Maintainability Symposium (RAMS), pages 1–6, 2010. doi:10.1109/RAMS.2010.5448044.
- 19 J. W. McPherson. Reliability Physics and Engineering: Time-To-Failure Modeling. Springer, Cham, 3rd edition, 2019.
- 20 Kamal Medjaher, Diego Alejandro Tobon-Mejia, and Noureddine Zerhouni. Remaining Useful Life Estimation of Critical Components With Application to Bearings. *IEEE Transactions on Reliability*, 61(2):292–302, 2012. doi:10.1109/TR.2012.2194175.
- 21 Jiadong Meng, Changfeng Yan, Guangyi Chen, Yaofeng Liu, and Lixiao Wu. Health Indicator of Bearing Constructed by rms-CUMSUM and GRRMD-CUMSUM With Multifeatures of Envelope Spectrum. *IEEE Transactions on Instrumentation and Measurement*, 70:1–16, 2021. doi:10.1109/TIM.2021.3054000.

- 22 Alvaro Moreno and Matteo Mossio. Biological Autonomy: A Philosophical and Theoretical Enquiry. Springer, Dordrecht, 2015. doi:10.1007/978-94-017-9837-2.
- Ali Moshrefzadeh and Alessandro Fasana. The Autogram: An effective approach for selecting the optimal demodulation band in rolling element bearings diagnosis. *Mechanical Systems and Signal Processing*, 105:294–318, 2018. doi:10.1016/j.ymssp.2017.12.009.
- Stan Muñoz Gutiérrez and Franz Wotawa. A qualitative study on the applicability and optimization of spectral fault receptive fields for condition monitoring and prognosis, June 2025. Zenodo. doi:10.5281/zenodo.15660819.
- Danh Ngoc Nguyen, Laurence Dieulle, and Antoine Grall. Remaining Useful Lifetime Prognosis of Controlled Systems: A Case of Stochastically Deteriorating Actuator. *Mathematical Problems in Engineering*, 2015:1–16, 2015. doi:10.1155/2015/356916.
- You-Jin Park, Shu-Kai S. Fan, and Chia-Yu Hsu. A Review on Fault Detection and Process Diagnostics in Industrial Processes. Processes, 8(9), 2020. doi:10.3390/pr8091123.
- 27 Aisong Qin, Qinghua Zhang, Qin Hu, Guoxi Sun, Jun He, and Shuiquan Lin. Remaining Useful Life Prediction for Rotating Machinery Based on Optimal Degradation Indicator. Shock and Vibration, 2017:Article ID 6754968, 12 pages, 2017. doi:10.1155/2017/6754968.
- Yi Qin, Jiahong Yang, Jianghong Zhou, Huayan Pu, and Yongfang Mao. A new supervised multi-head self-attention autoencoder for health indicator construction and similarity-based machinery RUL prediction. *Advanced Engineering Informatics*, 56:101973, 2023. doi:10.1016/j.aei.2023.101973.
- 29 Robert B Randall. State of the art in monitoring rotating machinery-part 1. Sound and vibration, 38(3):14-21, 2004.
- Paul D Samuel and Darryll J Pines. A review of vibration-based techniques for helicopter transmission diagnostics. *Journal of Sound and Vibration*, 282(1):475–508, 2005. doi:10.1016/j.jsv.2004.02.058.
- 31 Abhinav Saxena, Jose Celaya, Edward Balaban, Kai Goebel, Bhaskar Saha, Sankalita Saha, and Mark Schwabacher. Metrics for evaluating performance of prognostic techniques. In 2008 International Conference on Prognostics and Health Management, pages 1–17, 2008. doi:10.1109/PHM.2008.4711436.
- 32 D. F. Shi, W. J. Wang, and L. S. Qu. Defect Detection for Bearings Using Envelope Spectra of Wavelet Transform. *Journal of Vibration and Acoustics*, 126(4):567–573, December 2004. doi:10.1115/1.1804995.
- Manula A. Somaratna and Alan W. Freeman. The receptive field construction of midget ganglion cells in primate retina. *Journal of Neurophysiology*, 133(1):268–285, 2025. doi: 10.1152/jn.00302.2024.
- Moncef Soualhi, Khanh T.P. Nguyen, Kamal Medjaher, Fatiha Nejjari, Vicenc Puig, Joaquim Blesa, Joseba Quevedo, and Francesc Marlasca. Dealing with prognostics uncertainties: Combination of direct and recursive remaining useful life estimations. *Computers in Industry*, 144:103766, 2023. doi:10.1016/j.compind.2022.103766.
- 35 George Vachtsevanos, Frank Lewis, Michael Roemer, Andrew Hess, and Biqing Wu. *Intelligent Fault Diagnosis and Prognosis for Engineering Systems*. Wiley, Hoboken, NJ, USA, 2006.
- 36 Biao Wang, Yaguo Lei, Naipeng Li, and Ningbo Li. A Hybrid Prognostics Approach for Estimating Remaining Useful Life of Rolling Element Bearings. *IEEE Transactions on Reliability*, 69(1):401–412, 2020. doi:10.1109/TR.2018.2882682.
- Weizhong Yan, Hai Qiu, and Naresh Iyer. Feature Extraction for Bearing Prognostics and Health Management (PHM)-A Survey. Technical report, Air Force Research Laboratory (AFRL/RXLMN), 2008.